UNIVERSITÀ DEGLI STUDI DI ROMA



FACOLTÀ DI INGEGNERIA

MASTER DI II LIVELLO IN INGEGNERIA E DIRITTO INTERNAZIONALE DELLO SPAZIO NEI SISTEMI DI COMUNICAZIONE, NAVIGAZIONE E SENSING SATELLITARE

"PRELIMINARY DESIGN OF AN ON-BOARD COLLISION AVOIDANCE SYSTEM FOR SICRAL CONSTELLATION"

Relatore

Ch.ma Prof.ssa Ernestina Cianca

Correlatori Candidato

Magg. GArn Antonio D'apolito Ten. GArn Roberto Errico Ten. GArn Giovanni Scognamiglio

INDEX

INTRODUCTION, 1

- CHAPTER 1 PRINCIPLES OF CONJUNCTION ASSESSMENT, 2
- CHAPTER 2 ON-BOARD CONJUNCTION ASSESSMENT, 6
 - 2.1 Sicral 2, 6
- CHAPTER 3 SOFTWARE ANALYSIS, 8
- CHAPTER 4 ON-BOARD COLLISION AVOIDANCE SENSOR ANALYSIS, 15
 - 4.1 Sensor, 15
 - 4.2 Configuration, 16
 - 4.3 Omnidirectional visibility, 18
 - 4.4 Simulation: E-W configuration, 19
 - 4.5 Simulation: N-S configuration, 28

CONCLUSIONS AND FUTURE APPLICATIONS, 35

REFERENCES, 36

INDEX OF THE ILLUSTRATIONS

T-1	1 1	•	1	\sim
H10	1-1.	primary	object	7
1 15.	1 1.	primary	object,	_

- Fig. 1-2: secondary object, 3
- Fig. 1-3: point of closest approach, 3
- Fig. 1-4: time of closest approach, 4
- Fig. 1-5: overall miss distance, 4
- Fig. 3-1: distribution of azimuth values (East), 10
- Fig. 3-2: distribution of azimuth values (West), 10
- Fig. 3-3: distribution of elevation values (East), 11
- Fig. 3-4: distribution of elevation values (East), 11
- Fig. 3-5: distribution of azimuth values (East, 1000 km range), 12
- Fig. 3-6: distribution of azimuth values (West, 1000 km range), 12
- Fig. 3-7: distribution of elevation values (East, 1000 km range), 13
- Fig. 3-8: distribution of elevation values (East, 1000 km range), 13
- Fig. 4-1: the AA-STR star tracker, 15
- Fig. 4-2: FOV in the E-W configuration, 16
- Fig. 4-3: FOV in the N-S configuration, 18
- Fig. 4-4: azimuth, elevation and range in the E-W configuration (EXPRESS-AMU1), 20
- Fig. 4-5: azimuth, elevation and range in omnidirectional visibility (EXPRESS-AMU1), 20
- Fig. 4-6: azimuth, elevation and range in the E-W configuration (EUTELSAT 36B), 22
- Fig. 4-7: azimuth, elevation and range in omnidirectional visibility (EUTELSAT 36B), 22
- Fig. 4-8: azimuth, elevation and range in the E-W configuration (EUTELSAT 7A), 24
- Fig. 4-9: azimuth, elevation and range in omnidirectional visibility (EUTELSAT 7A), 24
- Fig. 4-10: azimuth, elevation and range in the E-W configuration (KIZUNA), 26
- Fig. 4-11: azimuth, elevation and range in omnidirectional visibility (KIZUNA), 26
- Fig. 4-12: azimuth, elevation and range in the N-S configuration (EXPRESS-AMU1), 29
- Fig. 4-13: azimuth, elevation and range in omnidirectional visibility (EXPRESS-AMU1, 29
- Fig. 4-14: azimuth, elevation and range in the N-S configuration (EUTELSAT 36B), 31
- Fig. 4-15: azimuth, elevation and range in omnidirectional visibility (EUTELSAT 36B), 31
- Fig. 4-16: azimuth, elevation and range in the N-S configuration (KIZUNA), 33
- Fig. 4-17: azimuth, elevation and range in omnidirectional visibility (KIZUNA), 33

INDEX OF THE TABLES

- Tab. 2-1: Sicral 2 specifications, 7
- Tab. 3-1: statistical parameters of azimuth and elevation values (1000 km range), 14
- Tab. 4-1: AA-STR technical specifications, 15
- Tab. 4-2: azimuth and elevation of the sensors in the E-W configuration, 16
- Tab. 4-3: azimuth and elevation of the sensors in the actual configuration and N-S configuration, 17
- Tab. 4-4: omnidirectional visibility, 18
- Tab. 4-5: E-W configuration visibility, 19
- Tab. 4-6: E-W configuration visibility (EXPRESS-AMU1), 21
- Tab. 4-7: E-W configuration time of visibility under 100 km (EXPRESS-AMU1), 21
- Tab. 4-8: E-W configuration visibility (EUTELSAT 36B), 23
- Tab. 4-9: E-W configuration time of visibility under 100 km (EUTELSAT 36B), 23
- Tab. 4-10: E-W configuration visibility (EUTELSAT 7A), 25
- Tab. 4-11: E-W configuration time of visibility under 100 km (EUTELSAT 7A), 25
- Tab. 4-12: E-W configuration visibility (KIZUNA), 27
- Tab. 4-13: E-W configuration time of visibility under 100 km (KIZUNA), 27
- Tab. 4-14: N-S configuration visibility, 28
- Tab. 4-15: N-S configuration visibility (EXPRESS-AMU1), 30
- Tab. 4-16: N-S configuration time of visibility under 100 km (EXPRESS-AMU1), 30
- Tab. 4-17: N-S configuration visibility (EUTELSAT 36B), 32
- Tab. 4-18: N-S configuration time of visibility under 100 km (EUTELSAT 36B), 32
- Tab. 4-19: N-S configuration visibility (KIZUNA), 34
- Tab. 4-20: N-S configuration time of visibility under 100 km (KIZUNA), 34
- Tab. 5-1: comparison between the number of detecting satellites, 35
- Tab. 5-2: comparison between the tracking times for different ranges (in respect of the omnidirectional visibility), 35

INTRODUCTION

The increasing utility of space-derived information has transformed our lives, enabling us to look outward and better understand our own solar system and our place in the universe, or to look inward and increase our knowledge of the Earth. Corporations, national governments, international agencies and individual citizens now consistently rely on spacecraft-supported communication, navigation and timing, imagery and remote sensing information capabilities to conduct daily business. Space is no longer the domain of a struggle between superpowers, it has evolved and become a place of utility for all mankind. In this environment collision avoidance is becoming a crucial matter, playing a key role during the whole operative life of every spacecraft. The ever-increasing number of orbiting objects (not only the controlled ones) requires the capability to rapidly evaluate the risk of a collision and, if necessary, to manoeuvre in order to avoid it. A major collision would create much additional debris, so avoiding collisions benefits the whole space community. After the Iridium-Cosmos collision in early 2009, the Joint Space Operations Center of the U.S. Strategic Command began to conduct conjunction analyses for all operational spacecrafts in Earth orbit, regardless of ownership. Any prediction of a close approach or conjunction is immediately shared with the spacecraft owner/operator. The Combined Space Operations Center (CSpOC), located at Vandenberg Air Force Base, California, actively tracks all objects of 'softball size' (10cm) or larger in orbit, using the US Space Surveillance Network (SSN) as our primary detection suite of sensors. The SSN is comprised of ground radar and optical systems and some space-based sensors, such as the US Space- Based Space Surveillance (SBSS) spacecraft and Canada's Sapphire spacecraft.

CHAPTER 1

PRINCIPLES OF COLLISION AVOIDANCE AND CONJUNCTION ASSESSMENT

The term conjunction is used when the predicted miss distance between two on-orbit objects, or between a launch vehicle and an orbiting object, is smaller than a specified reporting volume. When we talk of *conjunction assessment* (CA) we refer to an iterative process whose purpose is to determine the Point of Closest Approach (PCA) and the Time of Closest Approach (TCA) of two tracked orbiting objects or between a tracked orbiting object and a launch vehicle (including spent stages) or payload.

• Primary object: the satellite asset, the launched object or the ephemeris file that is being screened for potential conjunctions;

In general, a CA analysis is characterized by some fundamental elements:

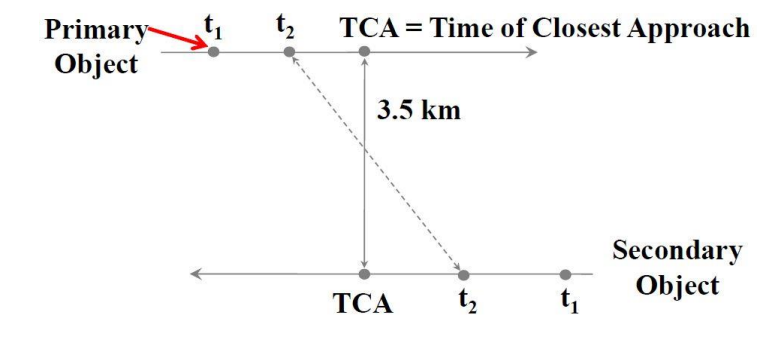


Fig. 1-1: primary object.

• Secondary object: all other satellite objects (e.g. Payloads, debris, analyst satellites, etc.) against which the primary object is being screened for potential conjunctions;

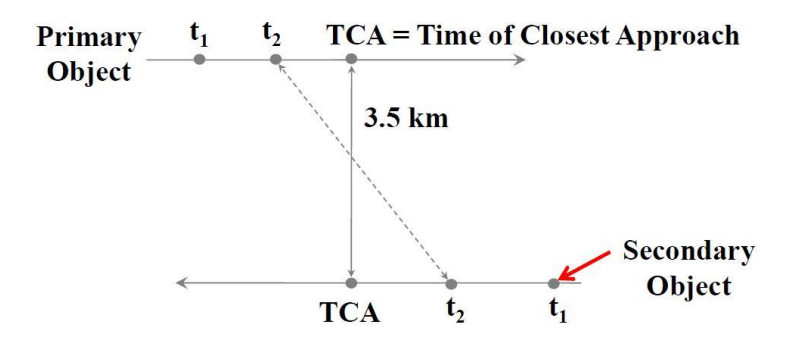


Fig. 1-2: secondary object.

• Point of closest approach (PCA): the point in each object's orbit where the magnitude of the relative position vector (i.e. miss distance) between the two objects is a minimum; the PCA occurs at the time of closest approach;

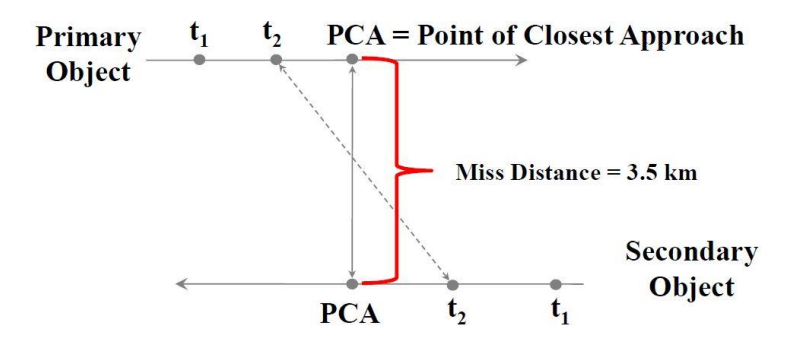


Fig. 1-3: point of closest approach.

• Time of closest approach (TCA): the time at which the minimum distance between two objects occurs; in particular, this occurs when the relative position vector is perpendicular to the relative velocity vector for the two objects involved in the conjunction;

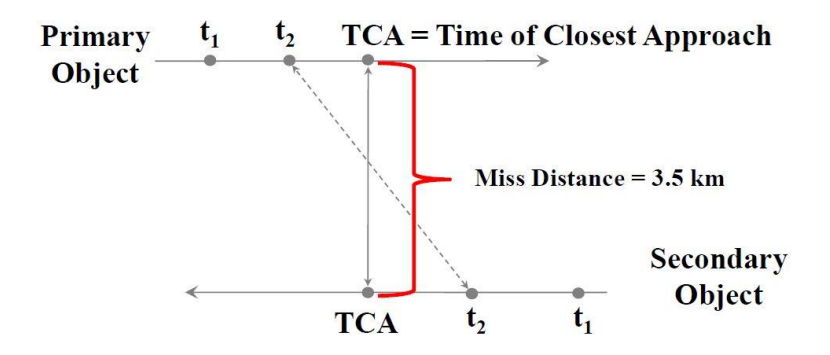


Fig. 1-4: time of closest approach.

• Overall miss distance: the PCA of one object relative to another; i.e. the minimum range, miss distance or relative position magnitude between two satellites at TCA.

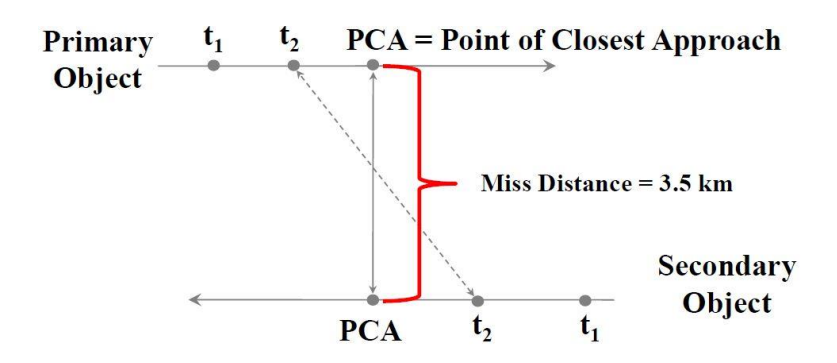


Fig. 1-5: overall miss distance.

When all these elements are known, we can proceed to evaluate the probability of collision (PC), that is the statistical measure of the likelihood that two objects' centres-of-mass will come within a specified distance of each other. The PC calculation requires covariance data (i.e. uncertainty data) on each object. This probability is usually expressed in scientific notation: large values are 1E-04 and higher, small values are 1E-06 and lower.

To determine if a satellite pair is a conjunction candidate, we define a screening volume, a spherical or ellipsoidal volume around the primary and secondary objects.

For the observation of the space environment two types of sensors are used:

- Radars, which provide three observables: range to target and two angles to target (azimuth and elevation);
- Optical sensors, which only report two angles: azimuth and elevation or right ascension and declination.

Most of these sensors are located on the Earth's surface and the entire CA process is exploited in the ground segment of a space mission.

CHAPTER 2

ON-BOARD CONJUNCTION ASSESSMENT

The increasing number of objects orbiting on the GEO ring is becoming a real menace for sensitive satellites. Not only collisions, but also intentional approaches aimed at intercepting telecommunications are eventualities which cannot be underestimated anymore. Therefore, is crucial to have the instruments and capabilities to promptly and successfully detect external threats before any damage occurs, allowing the satellite to operate proper anti-collision maneuvers. Such speed, reliability of tracking and readiness of execution can be only achieved with on-board sensors. The purpose of this work is to examine possible solutions to the request of a new collision avoidance sensor to carry onboard future satellites.

Since the purpose of this work is to evaluate new capabilities and technologies to implement on future satellites, to analyse a realistic scenario we have monitored Sicral 2 (an already launched and operative satellite) using software instruments over a period of time that goes from February 20 to March 21, 2020.

2.1 Sicral 2

Sicral 2 is a military telecommunication satellite with an advanced payolad operating in the UHF, SHF and EHF/Ka bands which serves the Italian and French departments of defense. Sicral 2 operates in GEO orbit and is located at 37° E longitude.

Sicral 2 provides strategical and tactical coverage for homeland security and abroad operations. Part of the transmissive capacity in possess of Italian and French MoD is offered to the armed forces of NATO allies.

NORAD ID	Int'l Code	Perigee	Apogee	Inclination
40614	2015-022B	35779.7 km	35808.8 km	0.0°
Period	Semi-major axis	Launch Date	Source	Launch site
1436.1	42165 km	April 26, 2015	France/Italy	French Guiana
minutes	42103 Km	April 20, 2013	(FRIT)	(FRGUI)

Tab. 2-1: Sicral 2 specifications.

CHAPTER 3

SOFTWARE ANALYSIS

The first step of our analysis consisted in the determination of the relative position of every GEO satellite in respect of Sicral 2 during the time window of interest.

A Keplerian orbit for Sicral 2 has been propagated from the TLE relative to our period of analysis (classified data) neglecting all the perturbative effects, since station keeping maneuvers are operated in order to guarantee a constant and stable pointing. In order to have a high number of close approaches to our satellite in the period of time of interest, we have made the assumption that all the objects in Geostationary belt did not perform any station keeping maneuver. By doing so, we simulated many uncontrolled space objects and debris entering the Geostationary box of Sicral 2.

To collect this data, we used the software AGI STK and then all the raw informations have been imported in MatLab to be refined and evaluated. To this purpose, we specifically developed a code which could derive the statistical parameters needed.

```
clc; clear all; close all;
load workspace tesi.mat
j=1;
for i=1:60483
    if (full(i,2)>90) && (full(i,2)<270)</pre>
        full a(j,:)=full(i,:);
    else
        if (full(i,2)>270)
             full_b(j,:)=full(i,:);
            full_b(j,2) = full(i,2) - 360;
        else
            full_b(j,:)=full(i,:);
        end
    end
    j=j+1;
az1=full a(any(full a\sim=0,2),:);
az2=full b(any(full b \sim = 0, 2),:);
for i=1:30267
    if (az1(i,4)<1000)
        az1_n(m,:)=az1(i,:);
    end
    m=m+1;
end
for i=1:30216
    if (az2(i,4)<1000)
```

```
az2_n(n,:)=az2(i,:);
else
end
n=n+1;
end

az_e=az1_n(any(az1_n~=0,2),:);
az_w=az2_n(any(az2_n~=0,2),:);

[m1,s1] = normfit(az_e(:,2));
[m2,s2] = normfit(az_w(:,2));
[m3,s3] = normfit(az_e(:,3));
[m4,s4] = normfit(az_w(:,3));
```

The variable called *full* is a *60483x4* matrix and it contains all the azimuth, elevation and range data of every GEO satellite collected in the time window. In the first column we have all the time samples (1 sample every 2 hours), in the second column the azimuth information, in the third column the elevation information and in the fourth column the range information.

The first *for* cycle creates two matrixes. The *full_a* matrix is a sub-matrix of *full* which contains all the azimuth values (and the correspondent elevation and range values) related to samples on the East side of Sicral 2 (only positive values). The *full_b* matrix is a sub-matrix of *full* which contains all the azimuth values (and the correspondent elevation and range values) related to samples on the West side of Sicral 2 (both positive and negative values). In the figures below we can see the distributions of azimuth and elevation values on the two sides of Sicral 2.

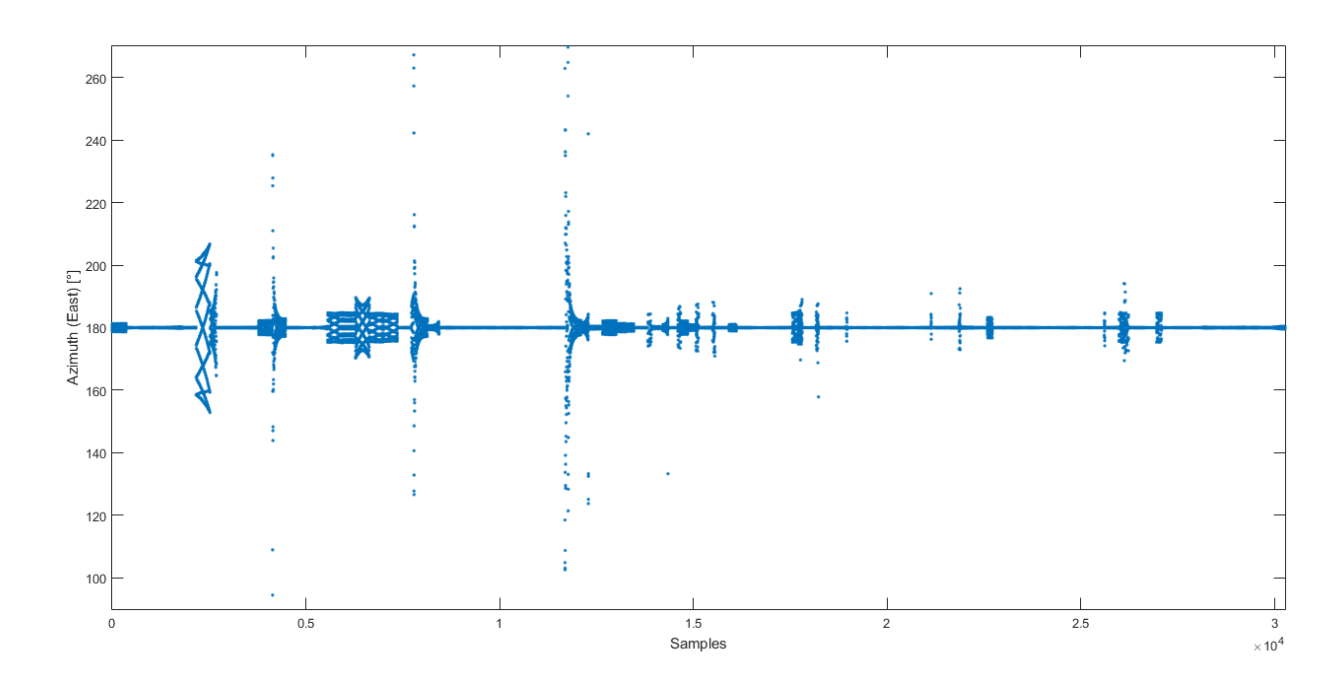


Fig. 3-1: distribution of azimuth values (East).

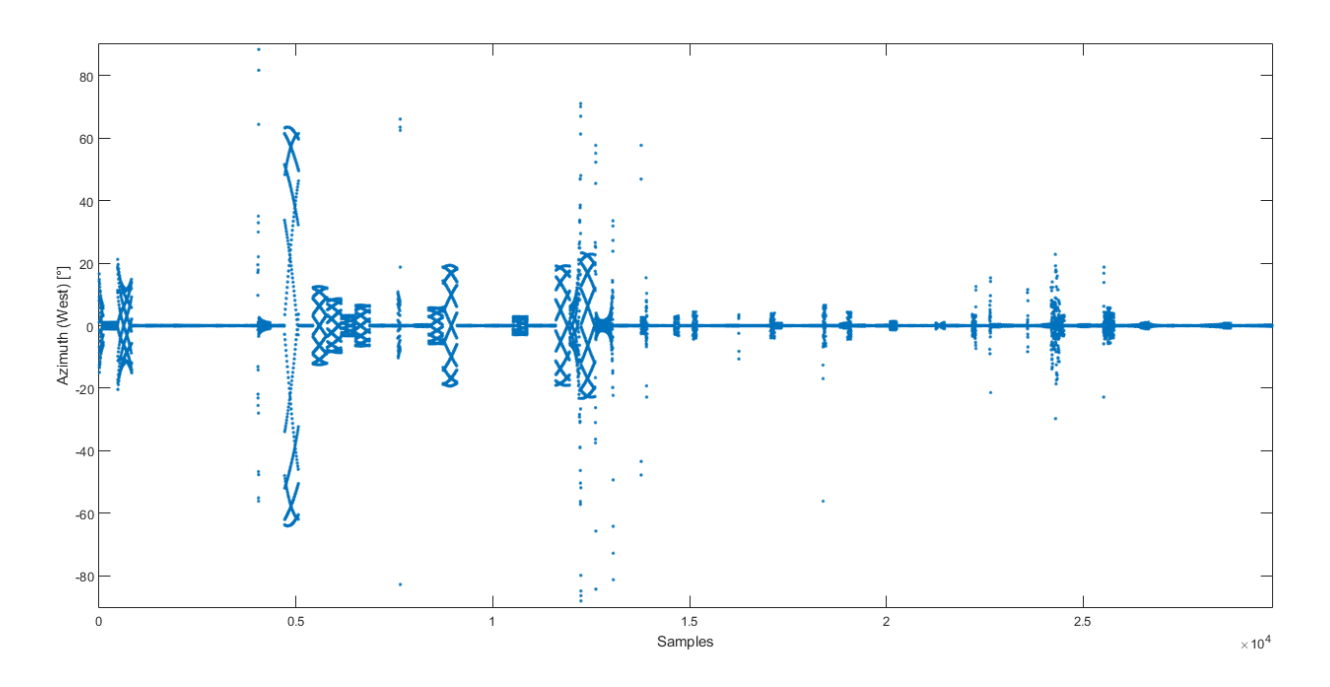


Fig. 3-2: distribution of azimuth values (West).

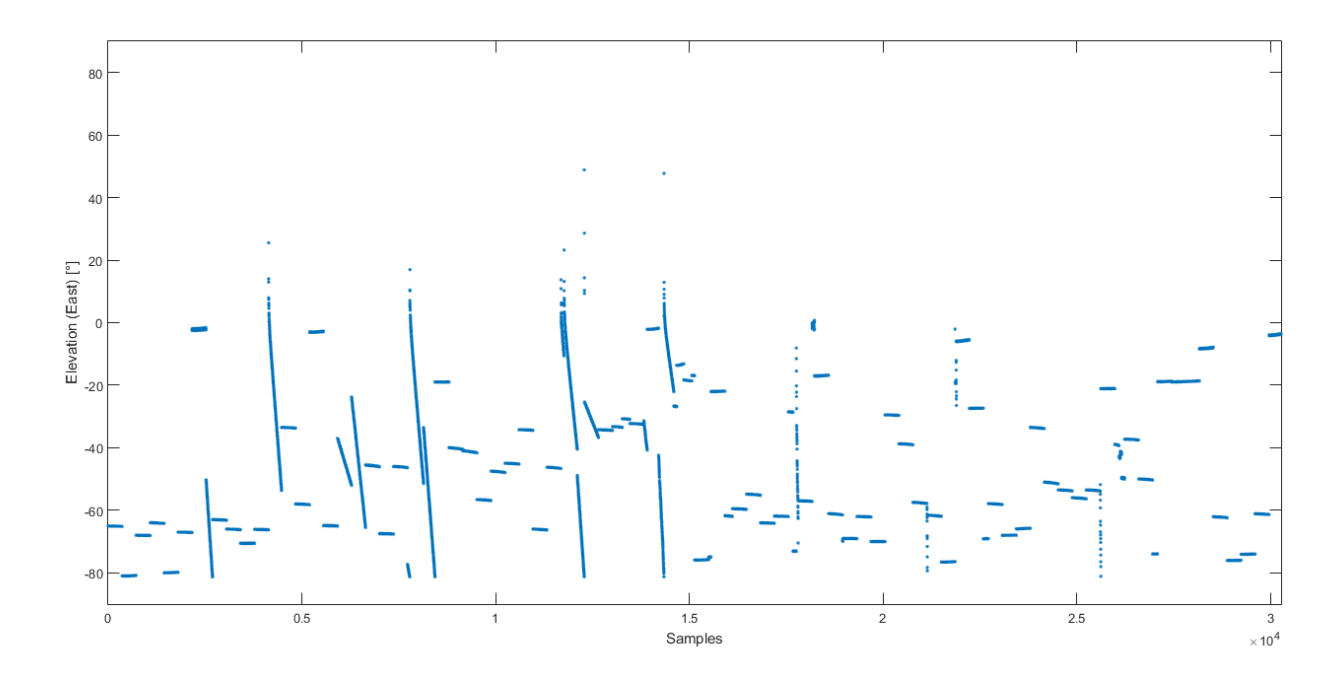


Fig. 3-3: distribution of elevation values (East).

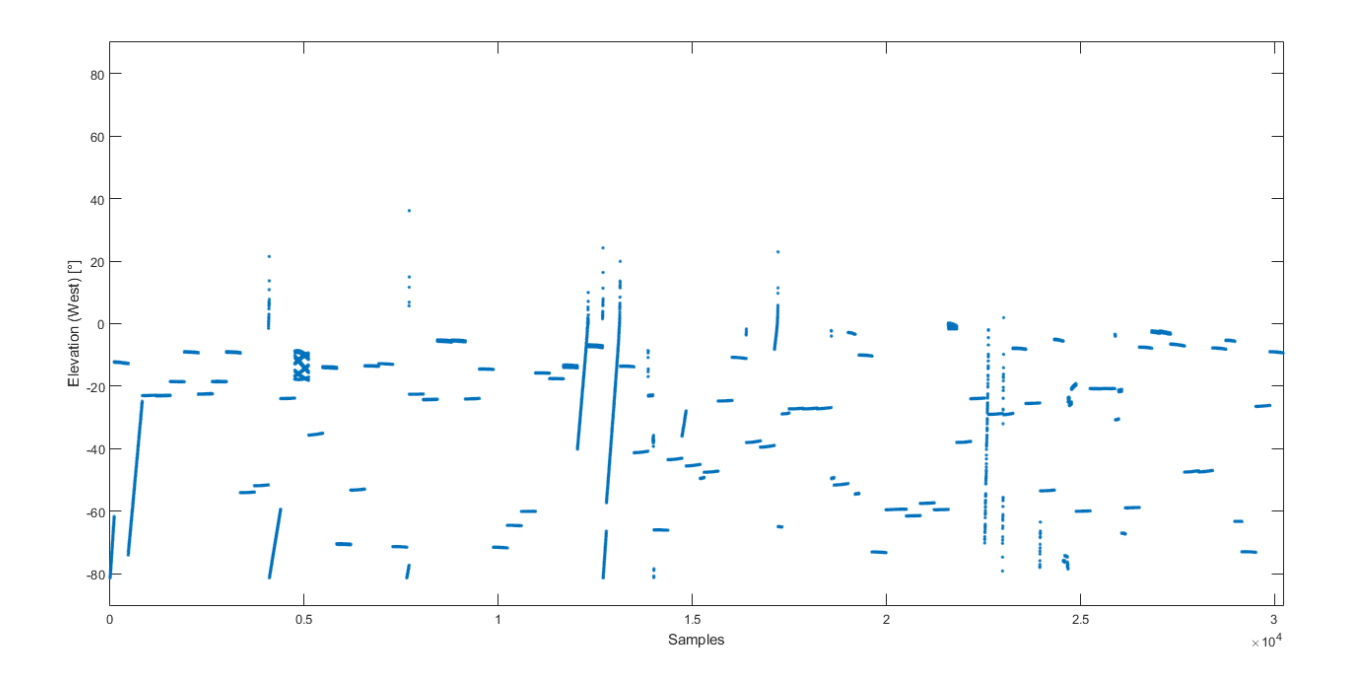


Fig. 3-4: distribution of elevation values (East).

The results shown above have been calculated for all the satellites on the GEO belt, but we are especially interested in the closest ones. In order to focus our analysis on these satellites, we added a "filter" portion in the code which discards satellites that are farther

than 1000 km from Sicral 2. This distance has been chosen because it is approximately the equivalent of 7 boxes, which can be considered an adequate safety range to start analysing uncontrolled space objects approaching. This selection has been operated with the two successive *for* cycles. The new results for azimuth and elevation are represented in the graphics hereafter.

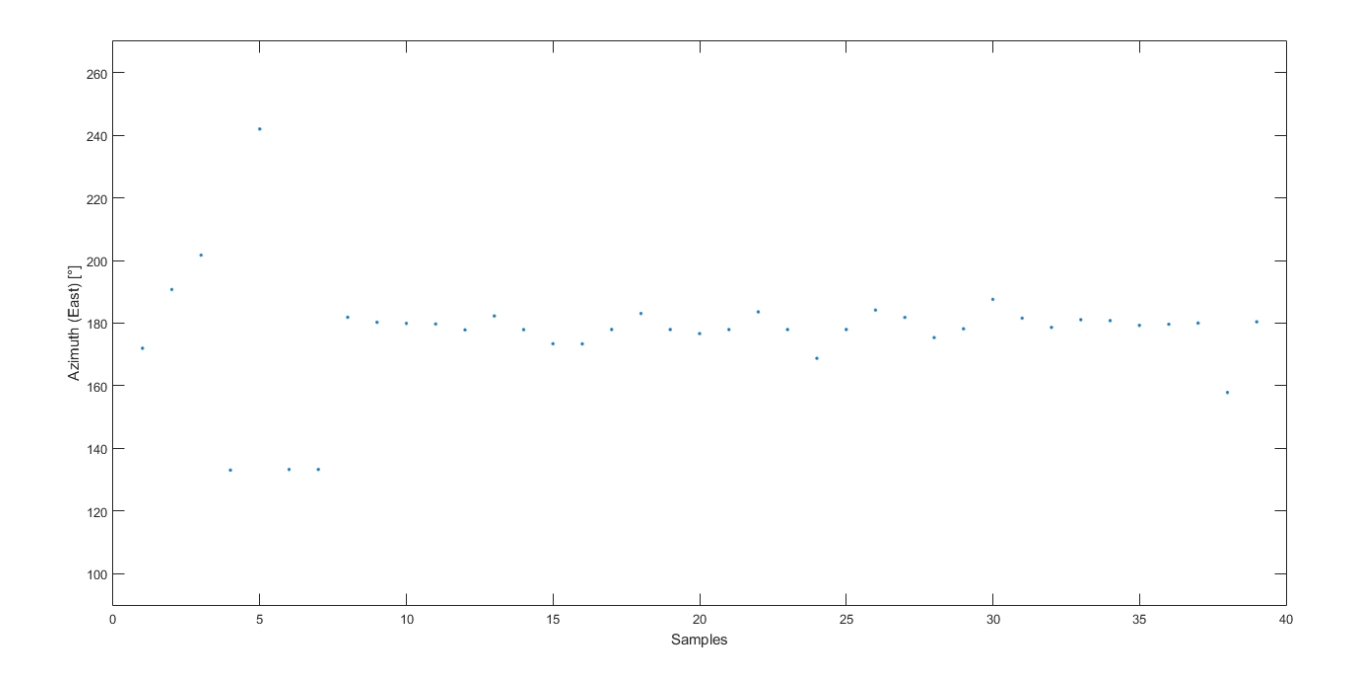


Fig. 3-5: distribution of azimuth values (East, 1000 km range).

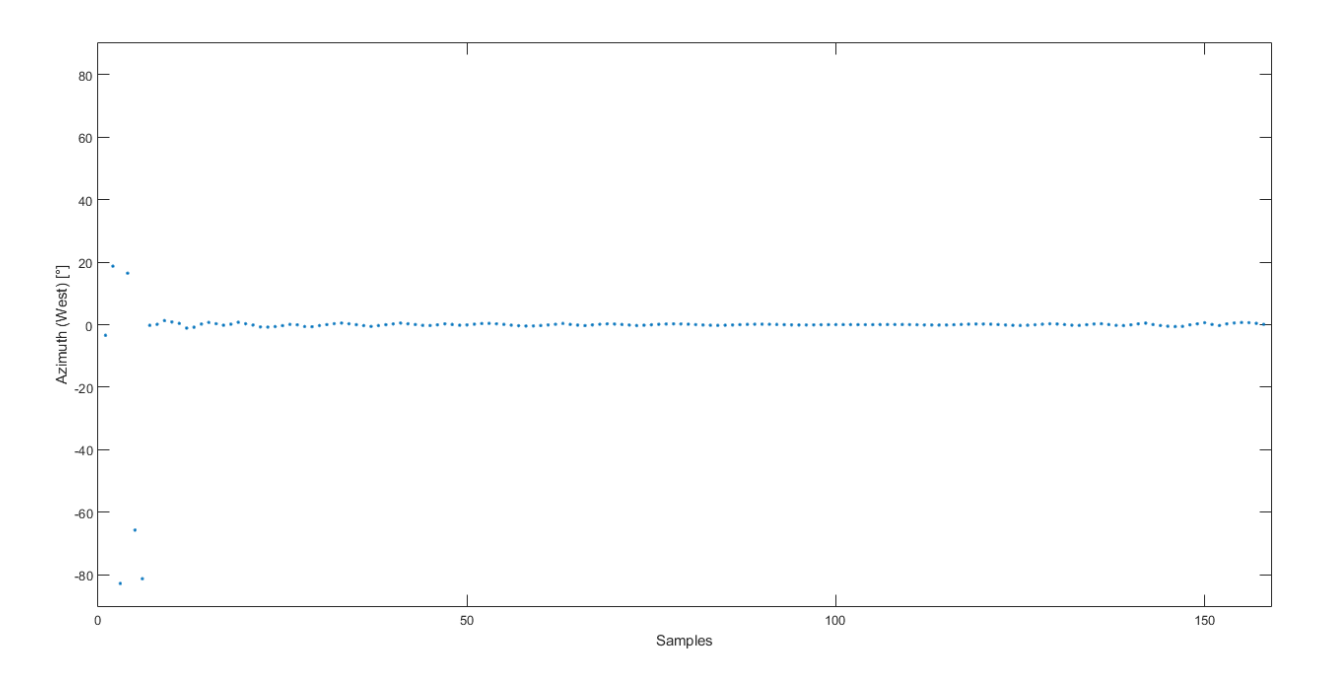


Fig. 3-6: distribution of azimuth values (West, 1000 km range).

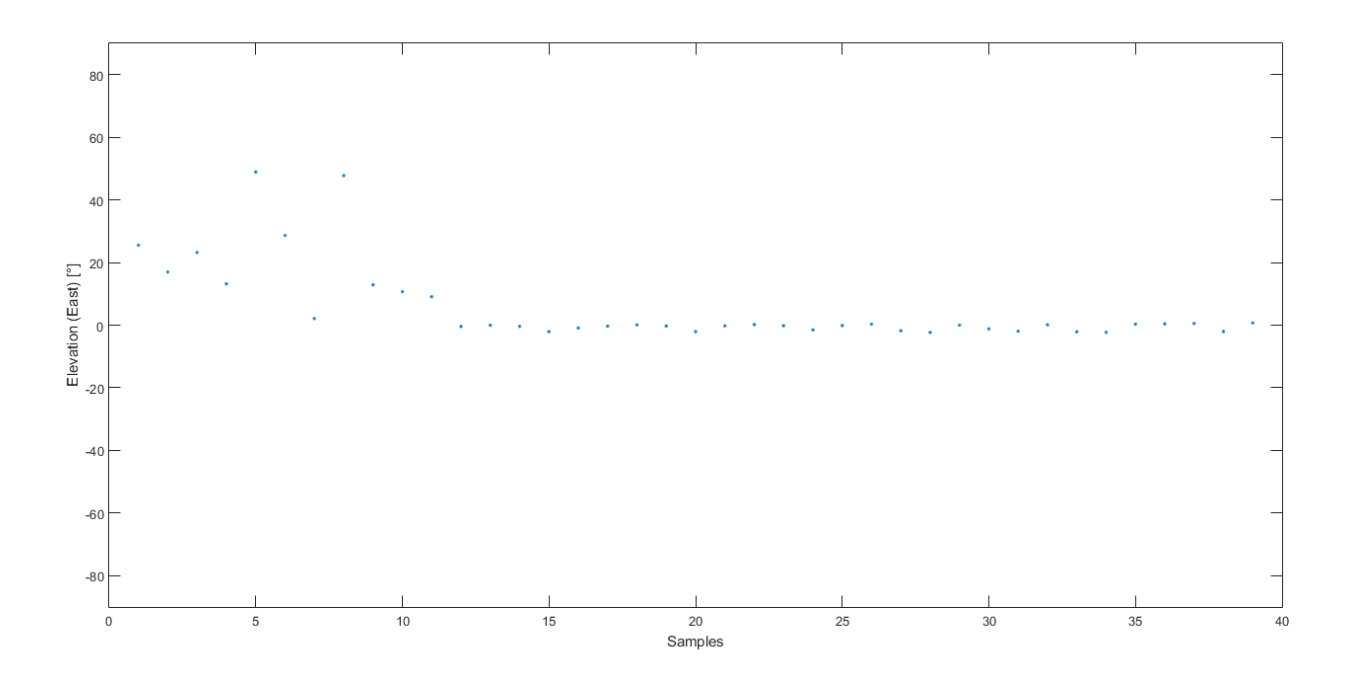


Fig. 3-7: distribution of elevation values (East, 1000 km range).

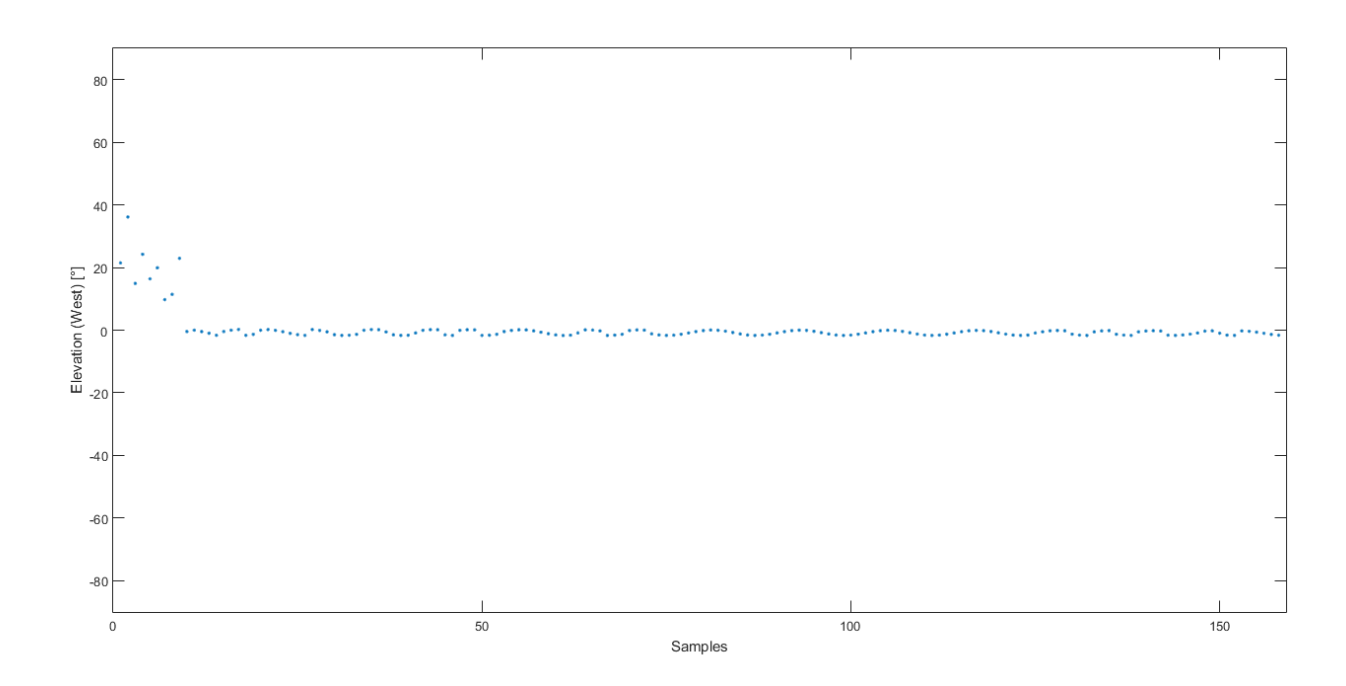


Fig. 3-8: distribution of elevation values (East, 1000 km range).

Once we have reduced the field of dangerous satellite, we proceeded with the estimate of the statistical parameters of these distributions. The *normfit* function computes the mean value and the standard deviation of an array. In this case, these statistical parameters have been found for the columns containing the azimuth and elevation values.

	Mean	Standard deviation
Azimuth (East)	177.5°	17.5°
Elevation (East)	5.6°	12.9°
Azimuth (West)	-1.2°	10.8°
Elevation (West)	0.4°	5.1°

Tab. 3-1: statistical parameters of azimuth and elevation values (1000 km range).

As a result of this analysis, we can infer that to properly implement these capabilities we need software and hardware instruments which can implement a FOV of at least 17.5° and a tracking range of approximately 1000 km. Such as technologies are already available on the market and one of them (the AA-STR star tracker sensor by Leonardo SpA) is currently equipped on Sicral 2, so it is a tested and space-ready technology. In addition, another possible solution is the software LAMPO by ARCA Dynamics. Tests conducted on the ground with this software on market-available star trackers show that it recognizes moving objects (especially GEO satellites, due to their dimensions) and outputs reliable data within a range of approximately 2000 km. This software processes the image data from the star tracker and detects all the moving objects, giving information on speed and relative distance. This information can be further processed by an on-board software in order to determine the orbit of the approaching objects and evaluate the chances of collision.

CHAPTER 4

ON-BOARD COLLISION AVOIDANCE SENSOR ANALYSIS

4.1 Sensor

The model of star tracker equipped on Sicral 2 is the AA-STR by Leonardo SpA, with a FOV of 20° and a CMOS APS sensor.



Fig. 4-1: the AA-STR star tracker.

AA-STR		
Detector	HAS APS	
FOV	20° x 20°	
Dynamic range	1.5 Mi to 5.5 Mi	
Number of Tracked	Up to 15	
Tracking rate	Up to 2°/sec	
Acquisition time	Lower than 9 seconds	
SEU tolerance	Up to 170000 protons/cm ² /sec	
Update rate	10 Hz, 8 Hz, 5 Hz, 4 Hz	

Tab. 4-1: AA-STR technical specifications.

4.2 Configuration

As a result of the software analysis produced with the software MatLab, in our scenario two different configurations have been considered for the star tracker sensors. To better evaluate the effectiveness of these configurations, they are compared with a software-simulated omnidirectional visibility.

In the first configuration (E-W configuration) the two sensors are located on the East and the West panels, oriented as follows:

	East sensor	West sensor
Azimuth	177.5°	-1.2°
Elevation	5.6°	0.4°

Tab. 4-2: azimuth and elevation in the E-W configuration.

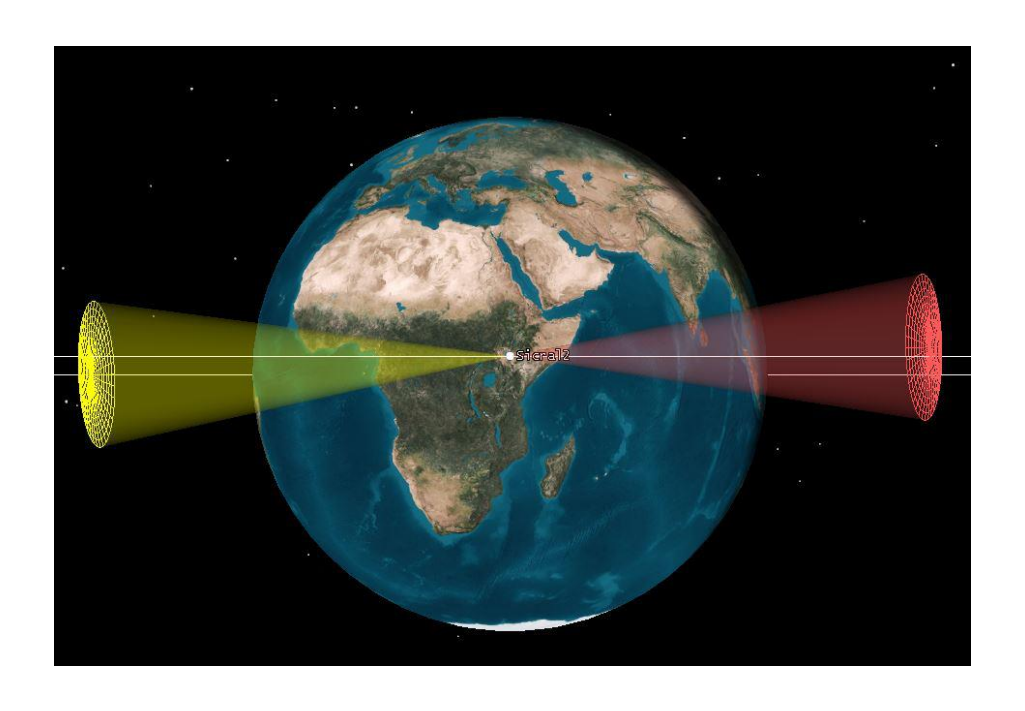


Fig. 4-2: FOV in the E-W configuration.

As we can see, these are the values resulted from the analysis in the previous chapter. In this configuration the Sun enters the FOV of the sensors, so they must be temporarily turned off to avoid potential damages.

The second configuration (N-S configuration) derives from the actual position of the star trackers on Sicral 2, in which the two sensors are located on the North and the South panels with an orientation perpendicular to the surface of the panels. To reach orientations as close as possible to the E-W configuration without allowing the Sun to enter the FOV of the sensors, we oriented the star trackers as follows:

		Actual configuration	N-S configuration
North sensor	Azimuth	-90°	-34°
Tioren sensor	Elevation	0°	0.4°
South sensor	Azimuth	90°	146°
South School	Elevation	0°	5.6°

Tab. 4-3: azimuth and elevation in the actual configuration and N-S configuration.

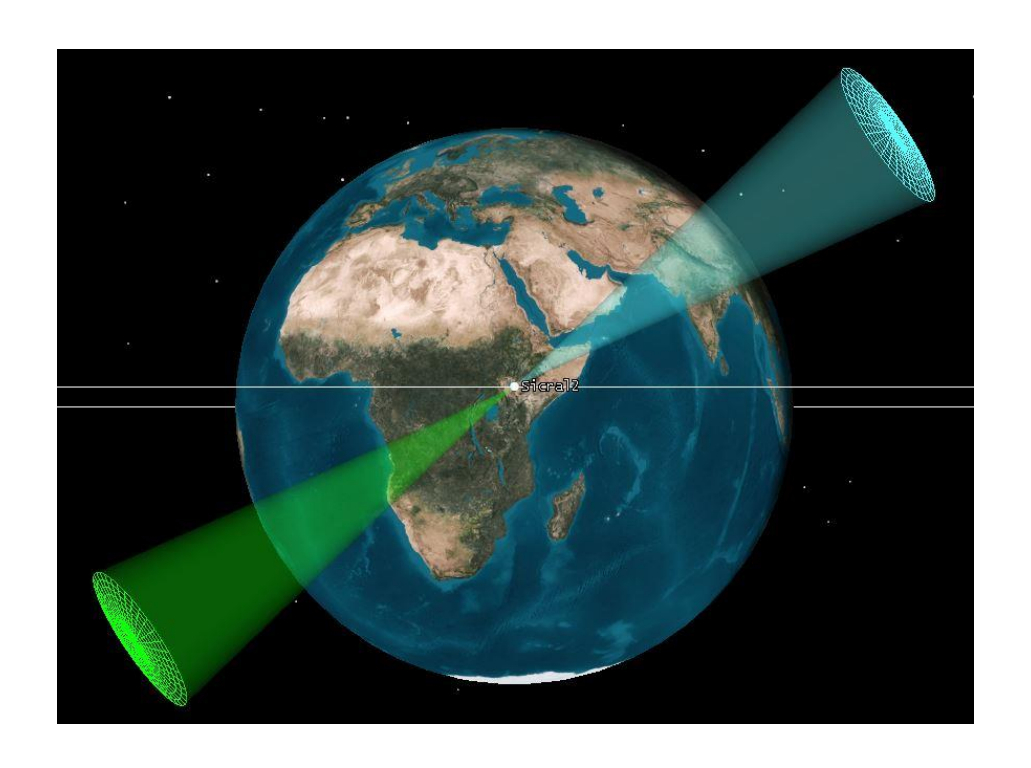


Fig. 4-3: FOV in the N-S configuration.

4.3 Omnidirectional visibility

In order to better evaluate the performances of the two configurations, a simulation of omnidirectional visibility (with a maximum range of 1000 km) has been conducted on Sicral 2. The results are shown in the table:

Detected satellites	Minimum distance	Maximum distance	Minimum time of observation	Maximum time of observation
28	8.3 km	999 km	152.8 sec	24 h

Tab. 4-4: omnidirectional visibility.

As we can see, the minimum detected distance is 8.3 km and it is reached by the object identified with the number 36101 in the NORAD catalogue, the operative satellite Eutelsat 36B (but uncontrolled in our simulation).

4.4 Simulation: E-W configuration

In this paragraph we will examine the E-W configuration. The results are shown in the table:

	Detected satellites	Minimum distance	Maximum distance	Minimum time of observation	Maximum time of observation
East sensor	7	28.4 km	999 km	65.6 sec	24 h
West sensor	6	55.8 km	999 km	391.8 sec	23.2 h

Tab. 4-5: E-W configuration visibility.

Now we will focus on the satellites which are seen by both sensors (i. e., which move across the box of Sicral 2).

• EXPRESS-AMU1 (NORAD ID: 41191)

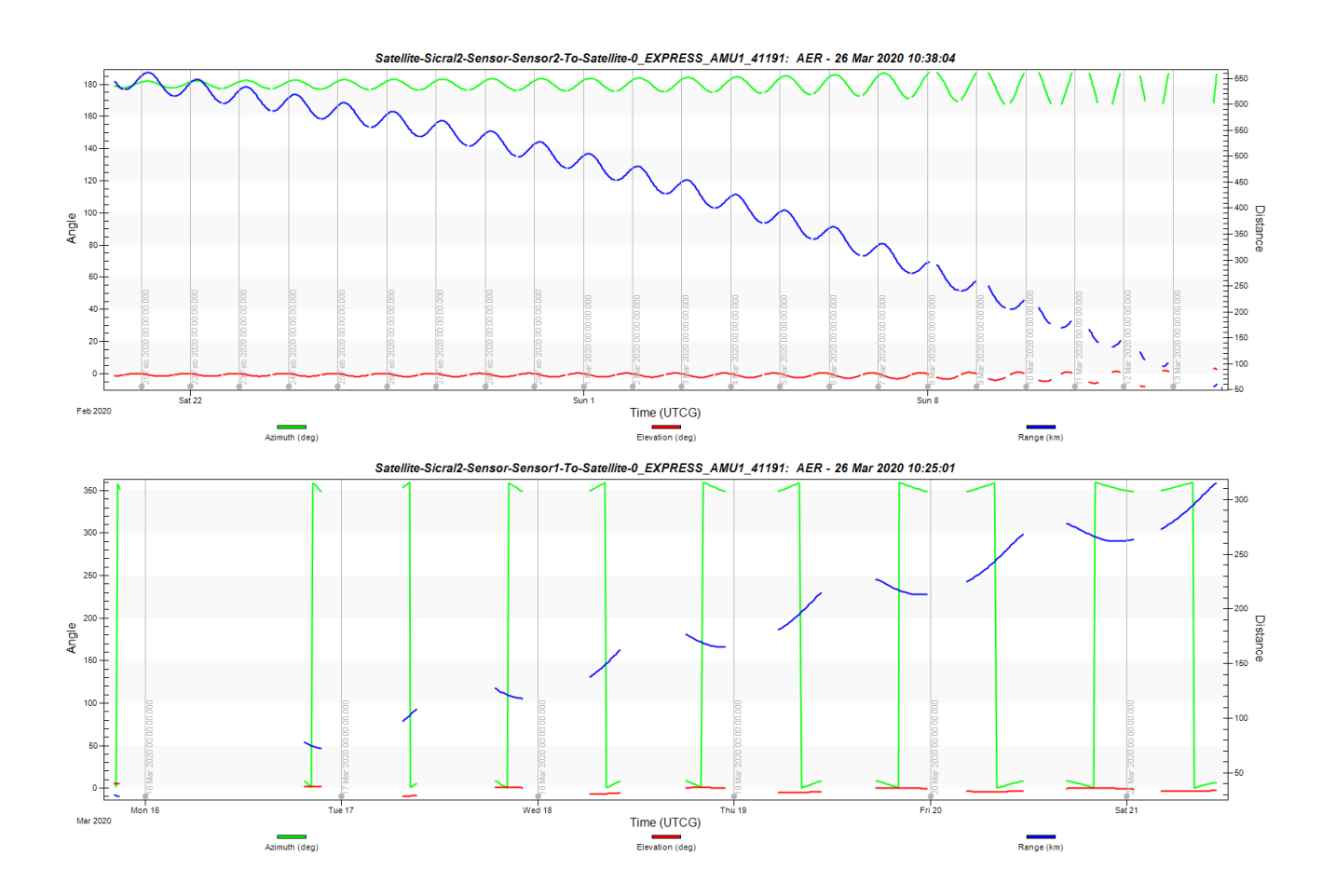


Fig. 4-4: azimuth, elevation and range in the E-W configuration.

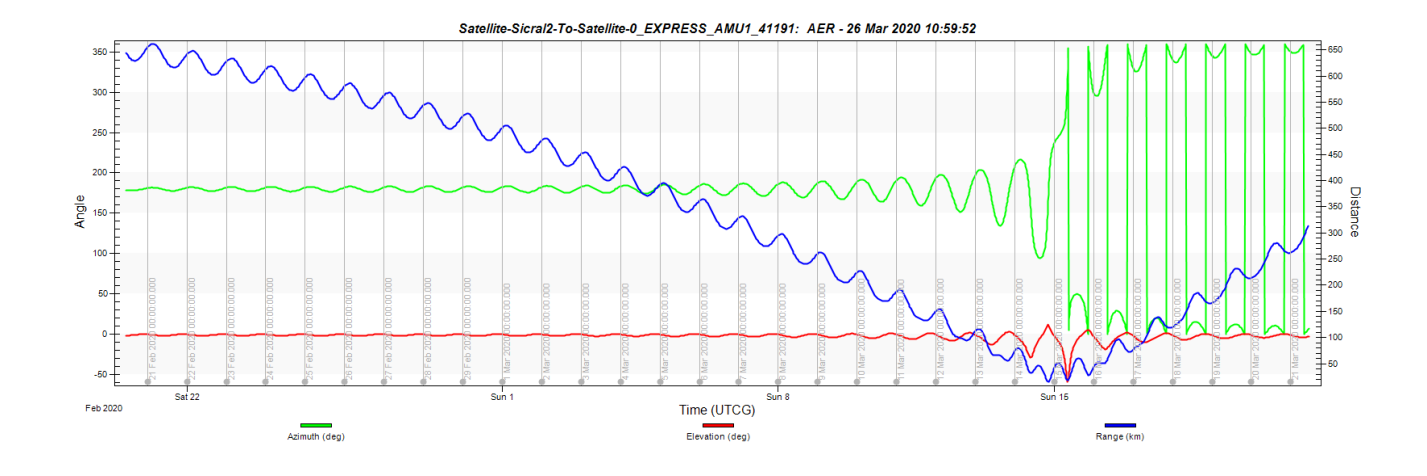


Fig. 4-5: azimuth, elevation and range in omnidirectional visibility.

	Minimum distance	Maximum distance	Minimum time of observation	Maximum time of observation
East sensor	28.4 km	315.8 km	2128 sec	8.3 h
West sensor	55.8 km	661.7 km	1.5 h	23.2 h
Omnidirectional	14.9 km	/	/	/

Tab. 4-6: E-W configuration visibility.

	Time of visibility under 100 km
East sensor	3 h
West sensor	3.5 h

Tab. 4-7: time of visibility under 100 km.

• EUTELSAT 36B (NORAD ID: 36101)

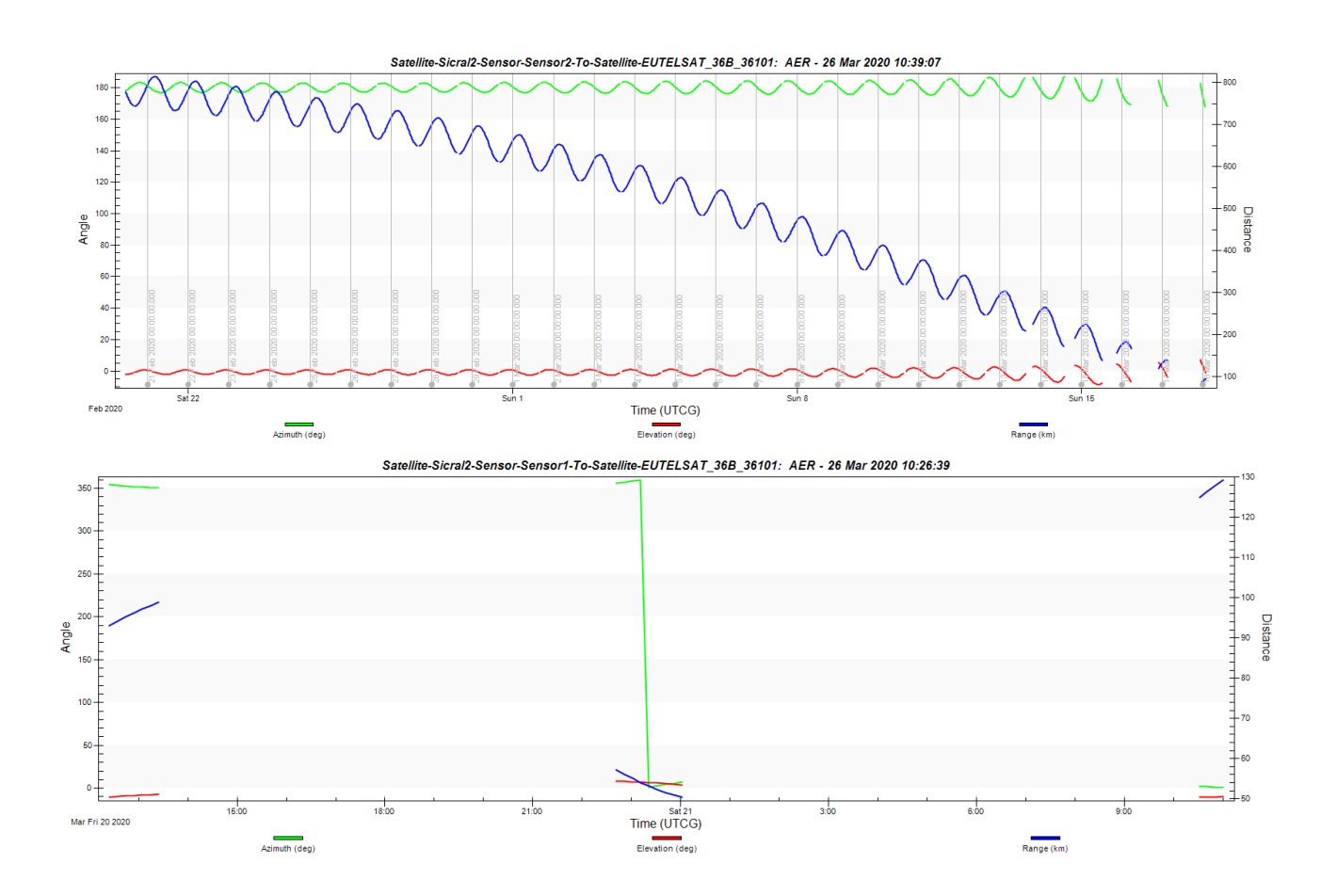


Fig. 4-6: azimuth, elevation and range in the E-W configuration.

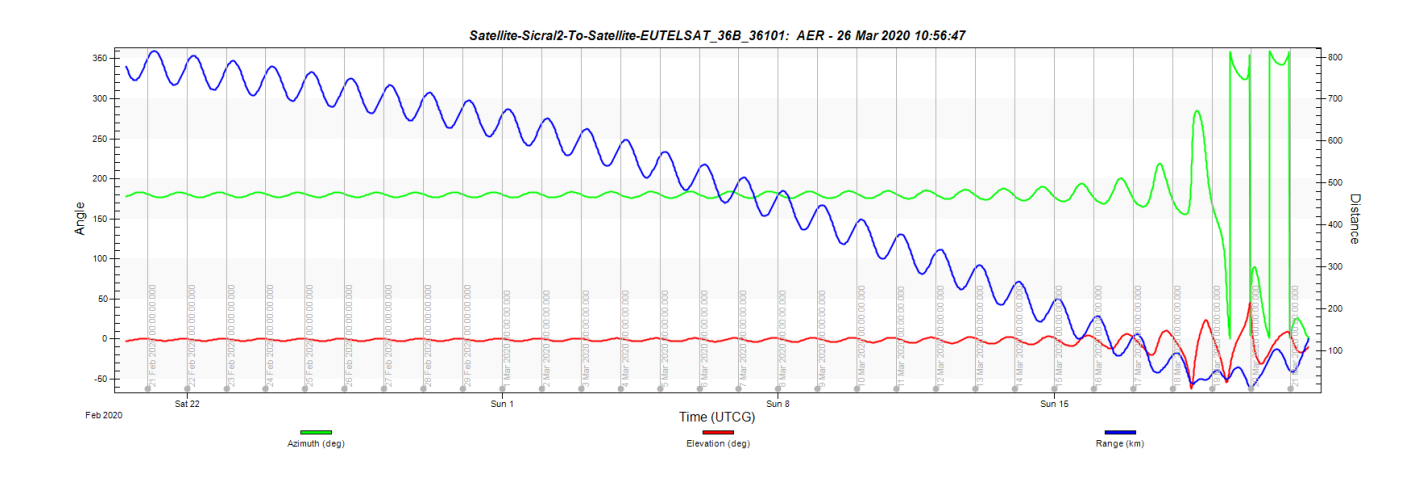


Fig. 4-7: azimuth, elevation and range in omnidirectional visibility.

	Minimum distance	Maximum distance	Minimum time of observation	Maximum time of observation
East sensor	50.4 km	129.4 km	1727 sec	1.3 h
West sensor	80.1 km	815.2 km	3.1 h	23.2 h
Omnidirectional	8.3 km	/	/	/

Tab. 4-8: E-W configuration visibility.

	Time of visibility under 100 km
East sensor	2.4 h
West sensor	3.1 h

Tab. 4-9: time of visibility under 100 km.

• EUTELSAT 7A (NORAD ID: 28187)

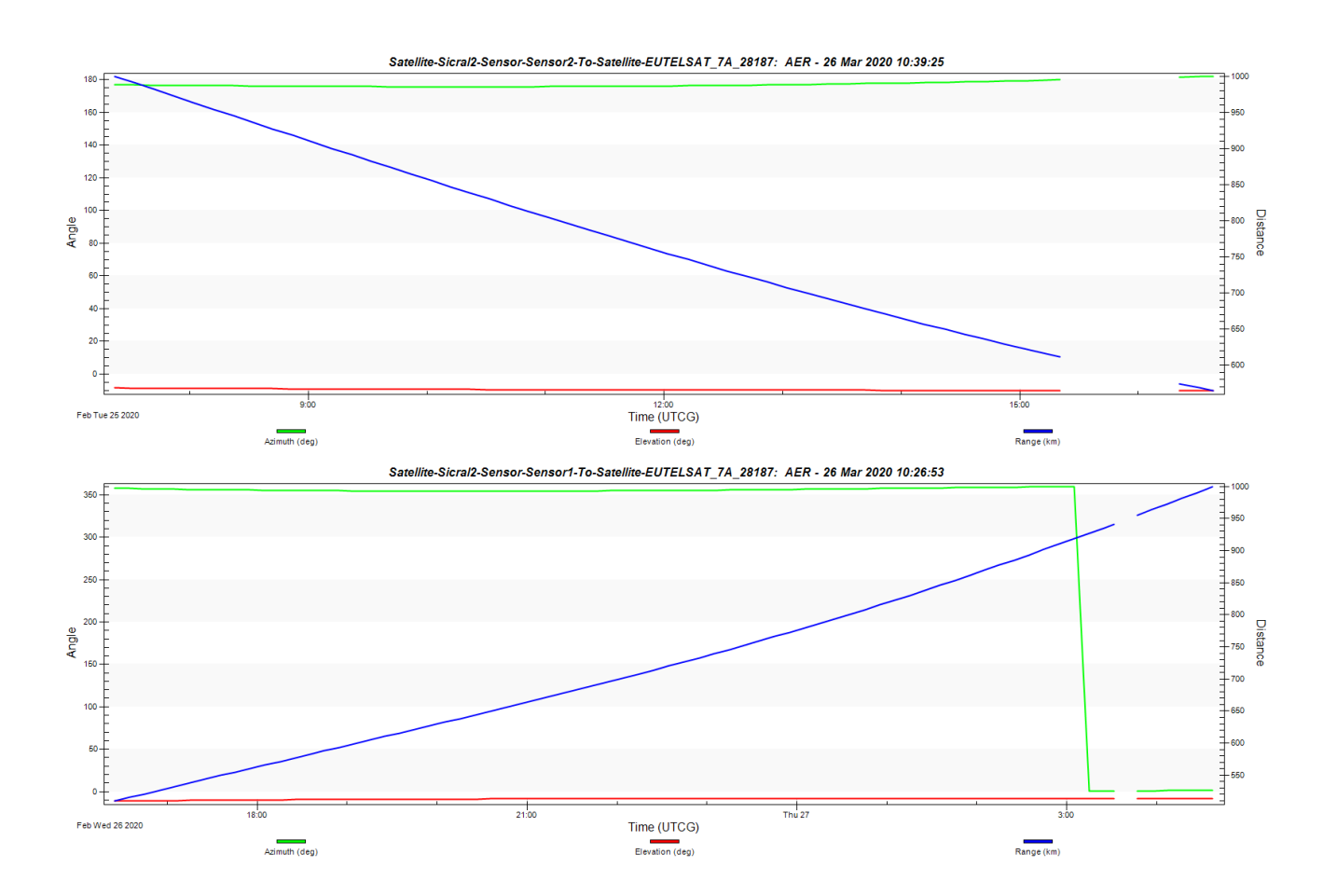


Fig. 4-8: azimuth, elevation and range in the E-W configuration.

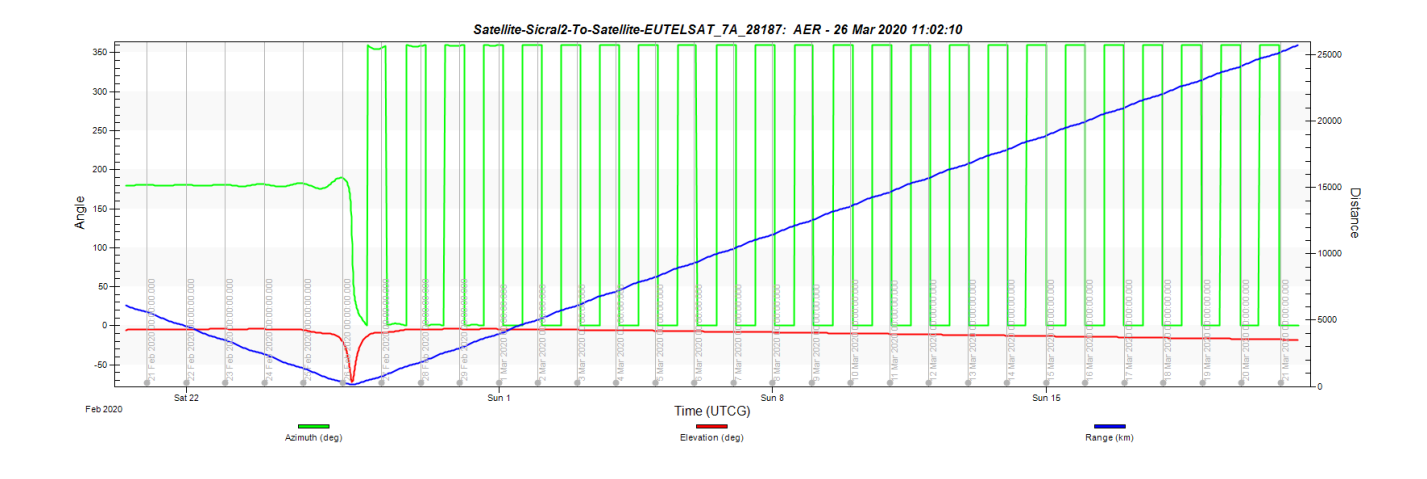


Fig. 4-9: azimuth, elevation and range in omnidirectional visibility.

	Minimum distance	Maximum distance	Minimum time of observation	Maximum time of observation
East sensor	509.6 km	999.9 km	3018 sec	11.1 h
West sensor	564.3 km	999.9 km	1013 sec	7.9 h
Omnidirectional	141.4 km	/	/	/

Tab. 4-10: E-W configuration visibility.

	Time of visibility under 100 km		
East sensor	/		
West sensor	/		

Tab. 4-11: time of visibility under 100 km.

• KIZUNA (NORAD ID: 32500)

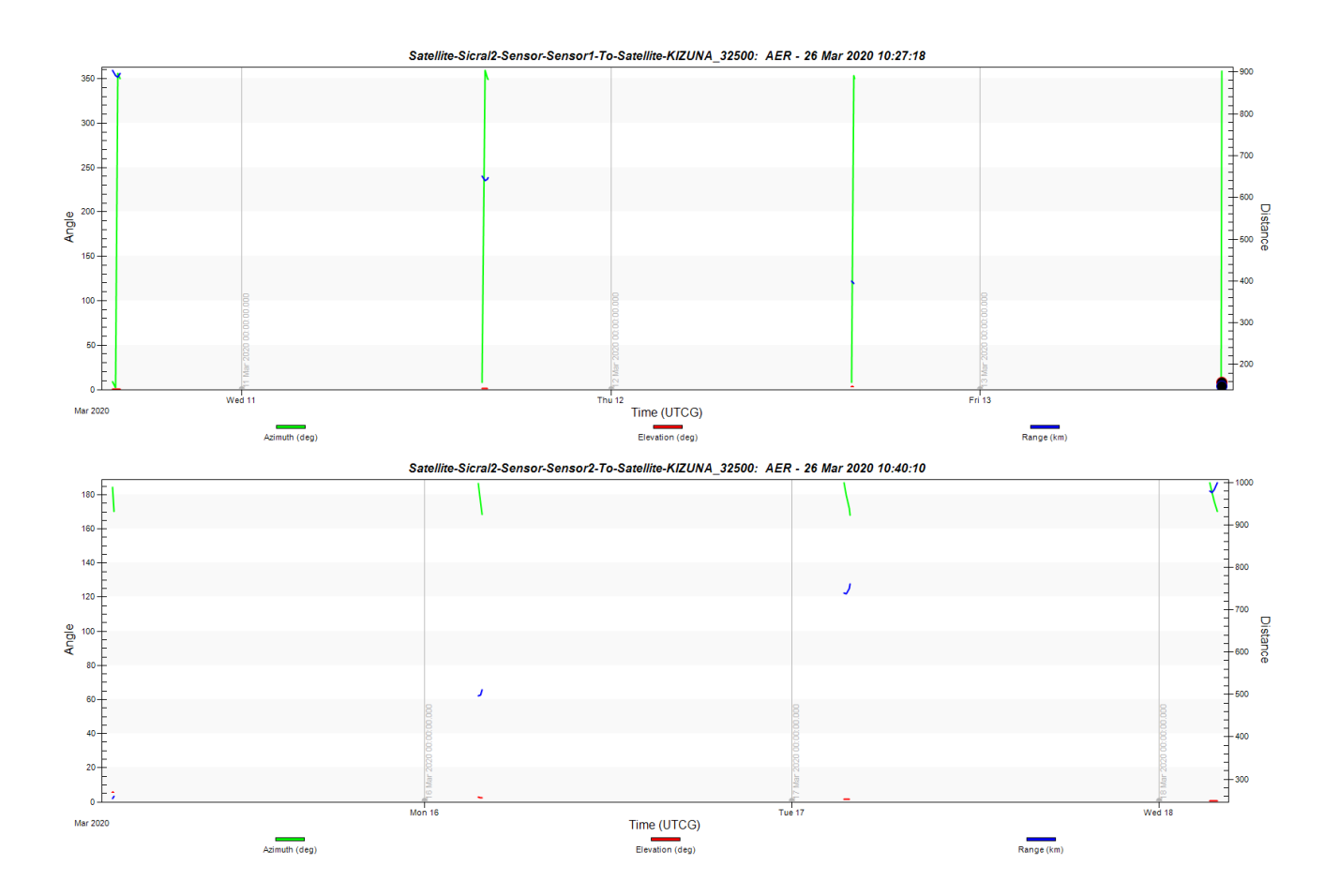


Fig. 4-10: azimuth, elevation and range in the E-W configuration.

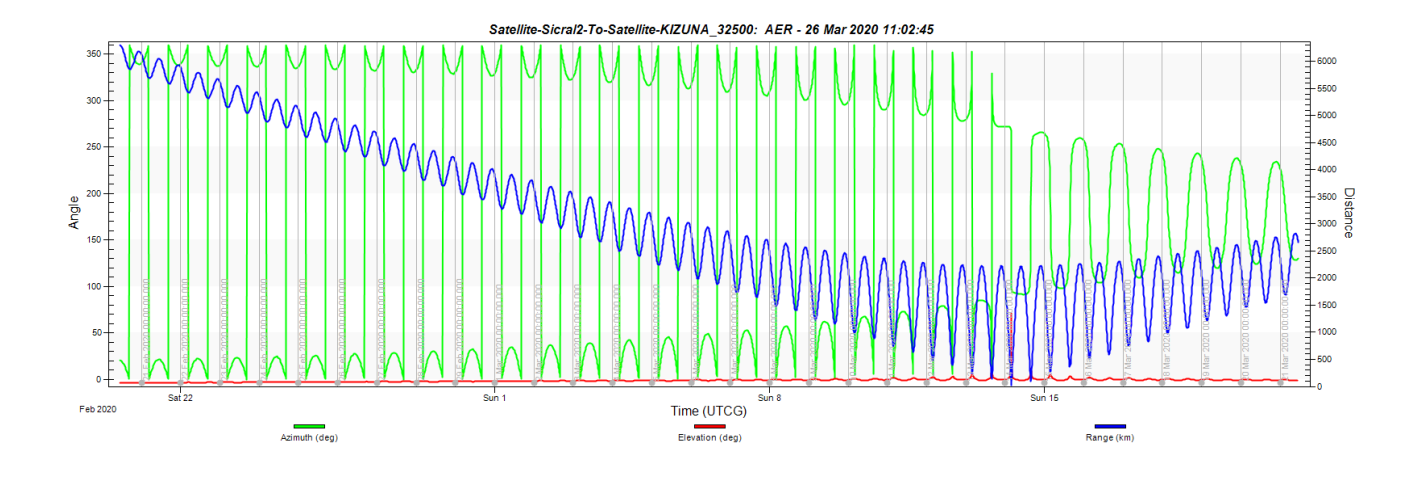


Fig. 4-11: azimuth, elevation and range in omnidirectional visibility.

	Minimum distance	Maximum distance	Minimum time of observation	Maximum time of observation
East sensor	147.8 km	904.7 km	65.6 sec	1885.6 sec
West sensor	253.9 km	999.9 km	391.8 sec	1809.9 sec
Omnidirectional	27.6 km	/	/	/

Tab. 4-12: E-W configuration visibility.

	Time of visibility	
	under 100 km	
East sensor	/	
West sensor	/	

Tab. 4-13: time of visibility under 100 km.

4.4 Simulation: N-S configuration

In this paragraph we will examine the N-S configuration. The results are shown in the table:

	Detected satellites	Minimum distance	Maximum distance	Minimum time of observation	Maximum time of observation
North sensor	3	28.8 km	999.9 km	309.5 sec	5.3 h
South sensor	4	51.8 km	999.9 km	784.1 sec	3.8 h

Tab. 4-14: N-S configuration visibility.

Now we will focus on the satellites which are seen by both sensors (i. e., which move across the box of Sicral 2).

• EXPRESS-AMU1 (NORAD ID: 41191)

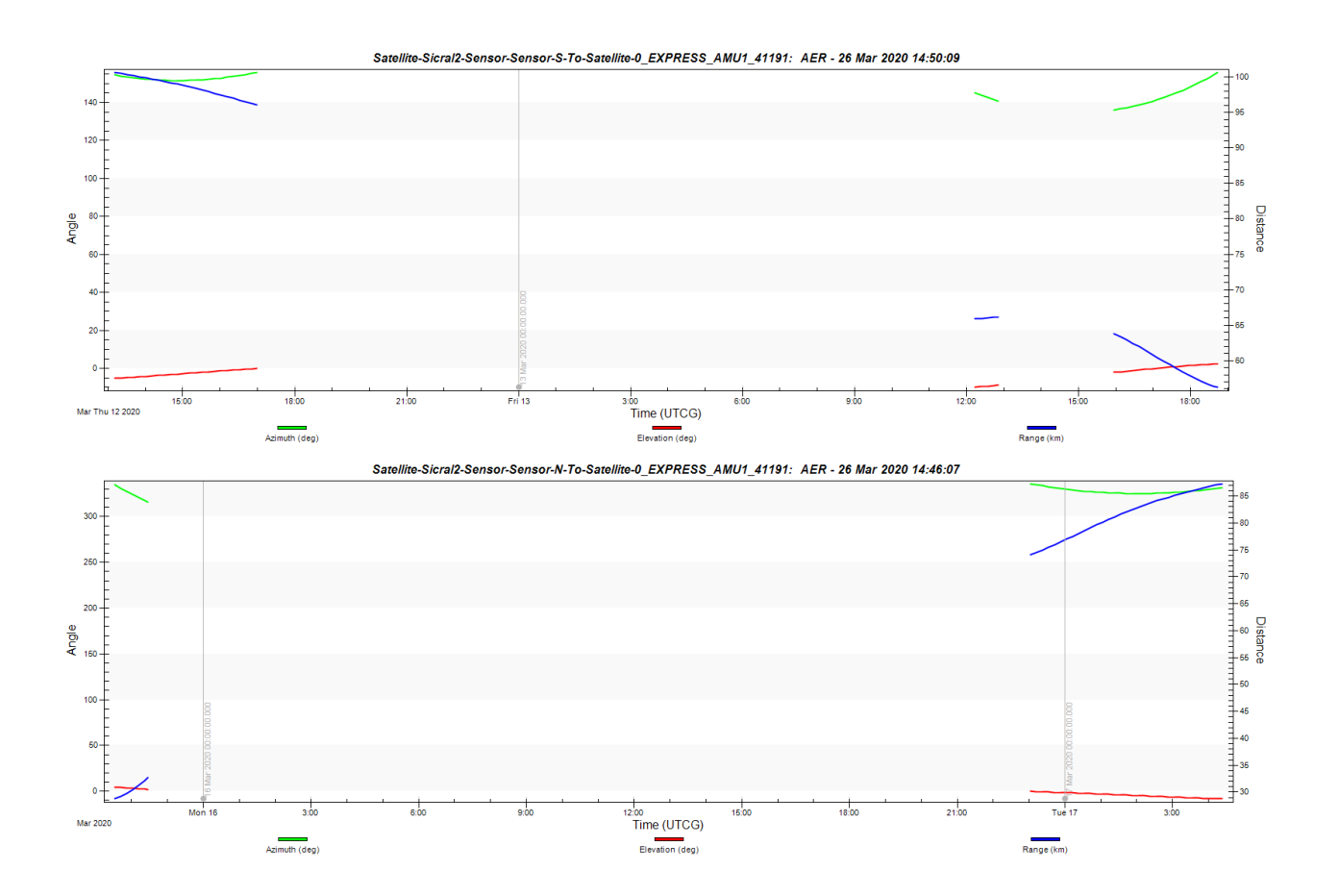


Fig. 4-12: azimuth, elevation and range in the N-S configuration.

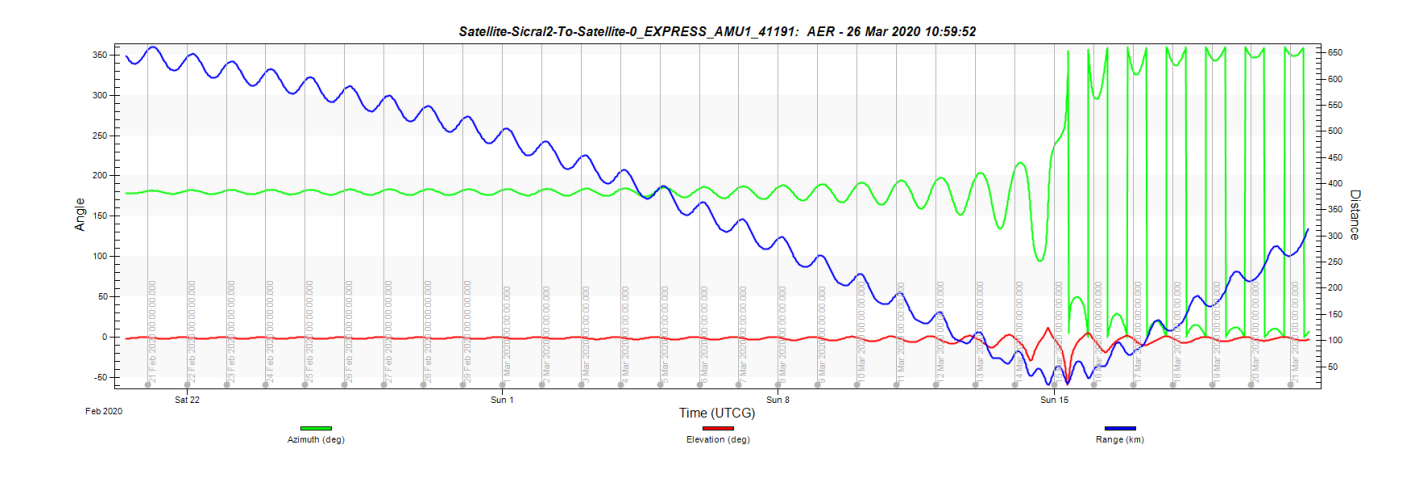


Fig. 4-13: azimuth, elevation and range in omnidirectional visibility.

	Minimum distance	Maximum distance	Minimum time of observation	Maximum time of observation
North sensor	28.8 km	87.3 km	3328.1 s	5.3 h
South sensor	56.2 km	100.7 km	784.2 s	1944.6 s
Omnidirectional	14.9 km	/	/	/

Tab. 4-15: N-S configuration visibility.

	Time of visibility			
	under 100 km			
North	6.2 h			
sensor	6.2 n			
South	6.5 h			
sensor	0.5 H			

Tab. 4-16: time of visibility under 100 km.

• EUTELSAT 36B (NORAD ID: 36101)

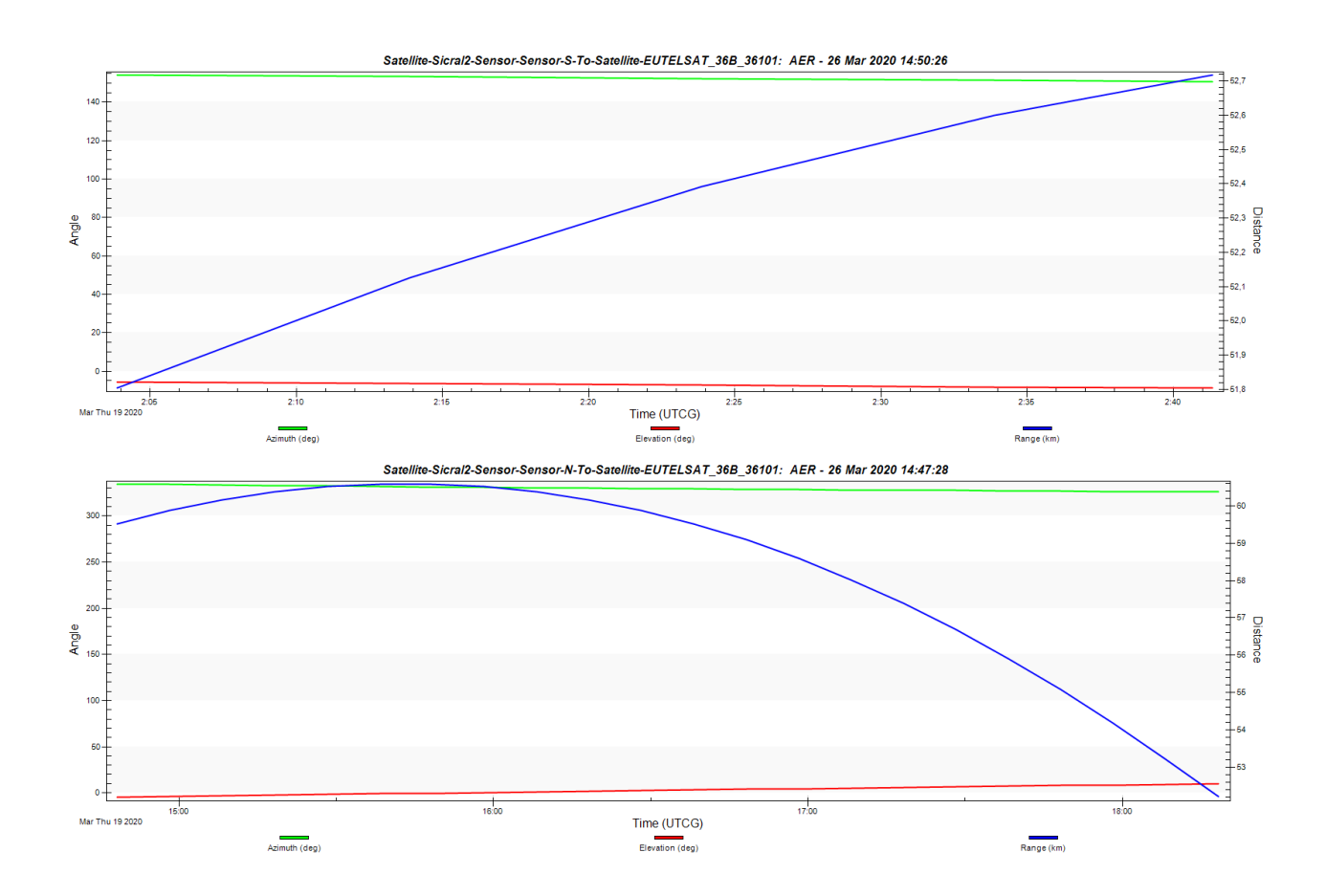


Fig. 4-14: azimuth, elevation and range in the N-S configuration.

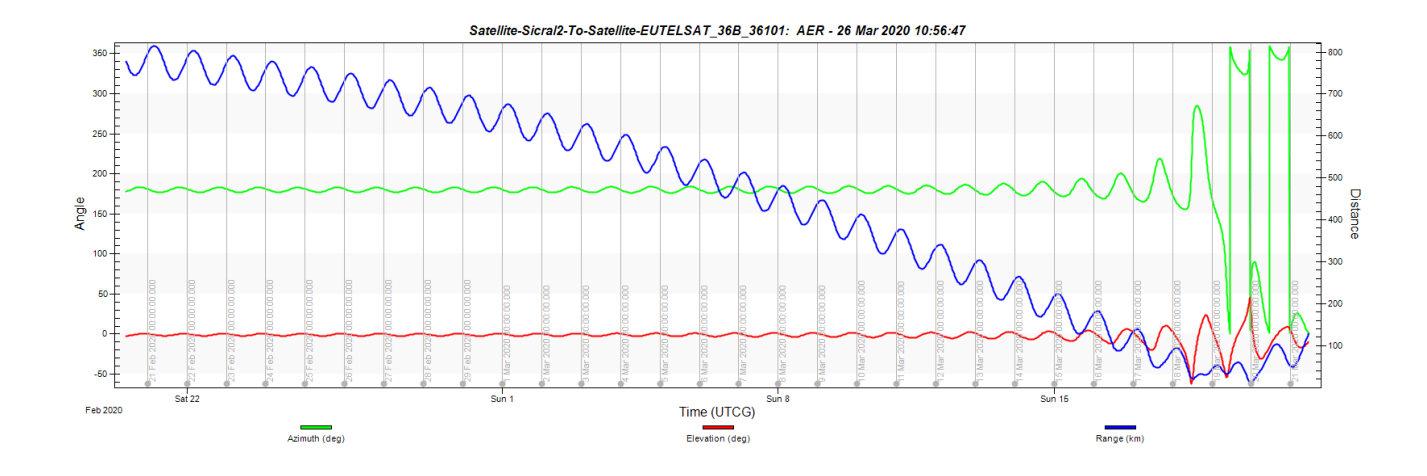


Fig. 4-15: azimuth, elevation and range in omnidirectional visibility.

	Minimum distance	Maximum distance	Minimum time of observation	Maximum time of observation
North sensor	52.2 km	60.6 km	3.5 h	3.5 h
South sensor	51.8 km	52.7 km	2247.5 s	2247.5 s
Omnidirectional	8.3 km	/	/	/

Tab. 4-17: N-S configuration visibility.

	Time of visibility			
	under 100 km			
North	3.5 h			
sensor	3.5 n			
South	2247.5 s			
sensor	22.7.6 5			

Tab. 4-18: time of visibility under 100 km.

• KIZUNA (NORAD ID: 32500)

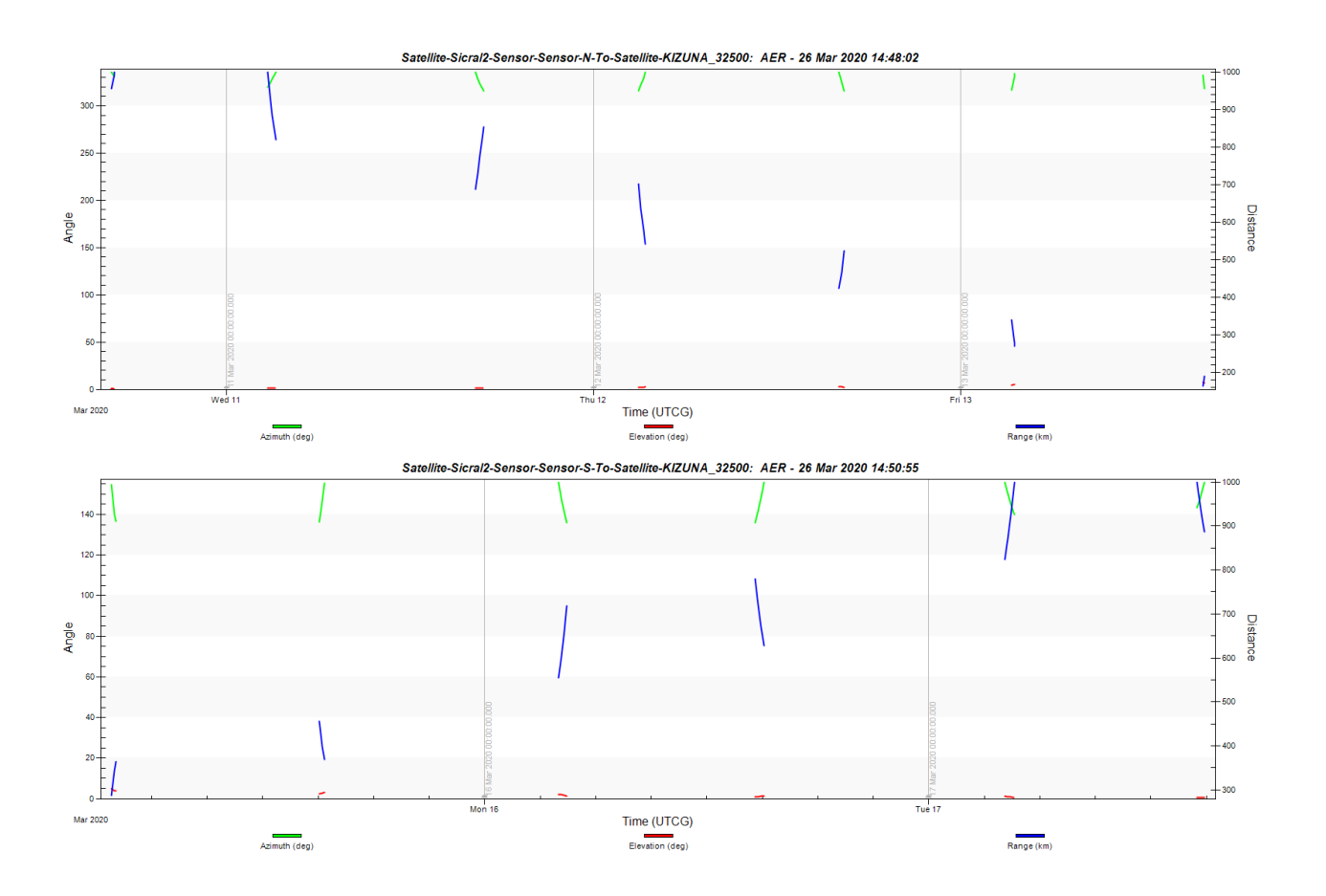


Fig. 4-16: azimuth, elevation and range in the N-S configuration.

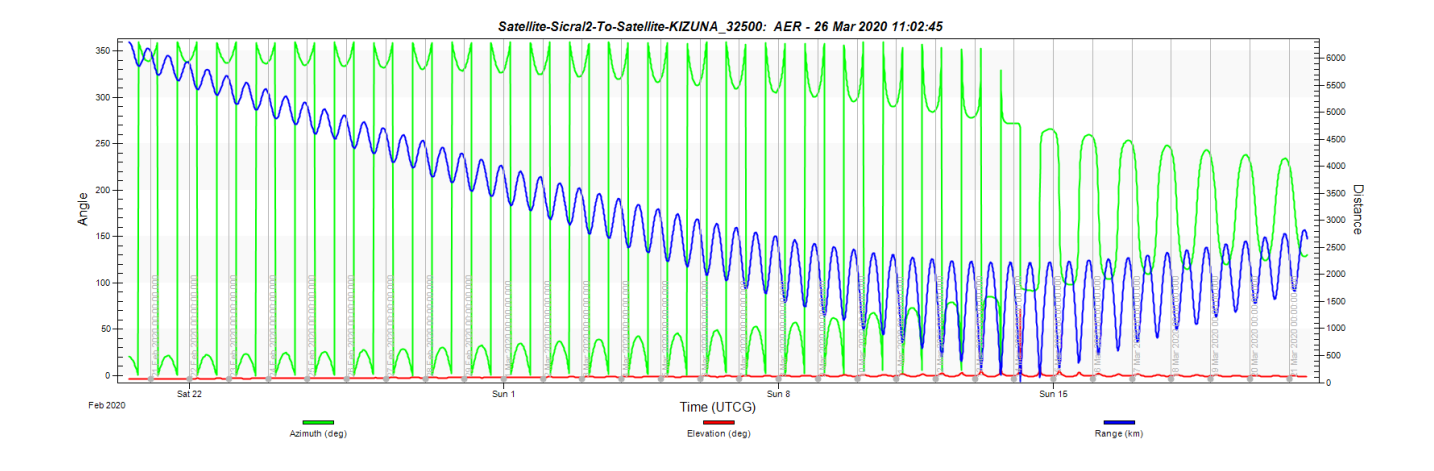


Fig. 4-17: azimuth, elevation and range in omnidirectional visibility.

	Minimum distance	Maximum distance	Minimum time of observation	Maximum time of observation
North sensor	163.0 km	999.9 km	309.5 s	1986.5 s
South sensor	286.9 km	999.9 km	784.2 s	1944.6 s
Omnidirectional	27.6 km	/	/	/

Tab. 4-19: N-S configuration visibility.

	Time of visibility	
	under 100 km	
North	/	
sensor	,	
South	/	
sensor	,	

Tab. 4-20: time of visibility under 100 km.

CONCLUSIONS AND FUTURE APPLICATIONS

The results obtained in the previous chapter show how the E-W configuration delivers better tracking performances than the N-S configuration. In particular, the star trackers in the E-W configuration are capable to detect more satellites and track them for longer periods, resulting in higher chances to calculate the orbit of the tracked object and assess the risk of a collision. A comparison between configuration can be seen in the tables:

	Omnidirectional	E-W configuration	N-S configuration
Detected satellites	28	g	4
(1000 km range)	20	,	7

Tab. 5-1: comparison between the number of detecting satellites.

	< 100 km	100 km – 200 km	>200km
E-W configuration	5.9 %	35.3 %	87.4 %
N-S configuration	8.2 %	0.45 %	0.3 %

Tab. 5-2: comparison between the tracking times for different ranges (in respect of the omnidirectional visibility).

The tables show that under 100 km range the N-S configuration outperforms the E-W configuration, because as satellites approach Sicral 2 they have higher values of azimuth and elevation. Above the 100 km distance, the E-W configuration is by far the best solution to track approaching satellites and is to be preferred.

In this thesis we have analysed one of the possible solutions to a collision avoidance sensor onboard a GEO satellites. Further analysis could be done by considering also active/passive RF or LASER sensors, or even a cluster of optical sensors (like our star trackers) to increase the FOV.

REFERENCES

- * ARCA Dynamics website, www.arcadynamics.com
- ❖ Telespazio website, www.telespazio.com
- ❖ Leonardo SpA, www.leonardocompany.com
- **S** ESA website, www.esa.int
- ❖ Collision Avoidance "Short Course", M.D. Hajduk, R.L. Frigm
- ❖ *Waste A handbook for management*, S. Hobbs, G. Stansbery, T. Matos de Carvalho